The quagmire of arrested development in tropical cyclones

Christopher J. Slocum [a] and John A. Knaff [a]

[a] *NOAA Center for Satellite Applications and Research, Fort Collins, Colorado*

Corresponding author: Chris Slocum, Christopher.Slocum@noaa.gov

Early Online Release: This preliminary version has been accepted for publication in *Weather and Forecasting*, may be fully cited, and has been assigned DOI 10.1175/WAF-D-22-0194.1. The final typeset copyedited article will replace the EOR at the above DOI when it is published.

ABSTRACT: Forty-eight hour intensity forecasts for Hurricane Pamela (2021) from numerical weather prediction models, statistical–dynamical aids, and forecasters were a major forecast bust with Pamela making landfall as a minor rather than major hurricane. From the satellite presentation, Pamela exhibited a symmetric pattern referred to as central cold cover (CCC) in the subjective Dvorak intensity technique. Per the technique, the CCC pattern is accompanied by arrested development in intensity despite the seemingly favorable convective signature. To understand forecast uncertainty during occurrences, central cold cover frequency from 2011–2021 is documented. From these cases, composites of longwave infrared brightness temperatures from geostationary satellites for CCC cases are presented and the surrounding tropical cyclone large-scale environment is quantified and compared with other tropical cyclones at similar latitudes and intensities. These composites show that central cold cover has a consistent presentation, but varies in the preceding hours for storms that eventually intensify or weaken. And, the synoptic-scale environment surrounding the tropical cyclone thermodynamically supports the vigorous deep convection associated with CCC. Finally, intensity forecast errors from numerical weather prediction models and statistical–dynamical aids are examined in comparison to similar tropical cyclones. This work shows that guidance struggles during CCC cases with intensity errors from these models being in the lowest percentiles of performance, particularly for 24- and 36-h forecasts.

Accepted for publication in *Weather and Forecasting*. DOI 10.1175/WAF-D-22-0194.1.

SIGNIFICANCE STATEMENT: The appearance of symmetric cold clouds near the center of developing tropical cyclones is most often associated with future intensification. This simple relationship is widely used by statistical tropical cyclone intensity forecast models. Here, we reexamine and confirm that one subjectively determined nighttime cold cyclone cloud pattern termed the "central cold cover" pattern in Vern Dvorak's seminal technique for estimating tropical cyclone intensity from infrared satellite images is indeed related to slow or arrested development, and represents a failure mode for these simple forecast models.

1. Introduction

At 1200 UTC on 11 October 2021, National Hurricane Center (NHC) forecasters predicted that tropical storm Pamela in the eastern North Pacific Ocean would intensify over the subsequent 48 hours as the storm neared Mexico's Pacific coast (Cangialosi 2021). Numerical weather prediction models (e.g., Global Forecast System, Hurricane Weather Research and Forecast, Hurricanes in a Multi-scale Ocean-coupled Non-hydrostatic, and Coupled Ocean–Atmosphere Mesoscale Prediction System-Tropical Cyclones) and statistical–dynamical guidance (e.g., Statistical Hurricane Intensity Prediction Scheme and Logistic Growth Equation Model) indicated that the storm's intensity would peak between 95 and 140 kt. Forecasters went with a 75 kt (1 kt $\approx$ 0.514 m s^{-1}) increase in the maximum sustained winds from the current intensity of 35 to 110 kt by 1200 UTC on 13 October, which meant that Pamela would make landfall as a major hurricane. However, Pamela's peak intensity never exceeded 65 kt prior to making landfall and succumbed to high deep-layer vertical wind shear (Cangialosi 2021). From the main environmental parameters associated with intensity change, Pamela was over 30 °C ocean water with low to moderate deep-layer vertical wind shear and fair middle-troposphere relative humidity — none of these storm environment factors had appreciable errors in numerical weather prediction model forecasts when compared with subsequent model analyses. The post-season analysis attributes Pamela's stalled intensification due to the entrainment of dry air (Cangialosi 2021), which implies that both the real-time guidance and final model analyses failed to resolve the dry air. However, model guidance and forecasters may have missed a nuance in the convective evolution within Pamela's inner core.

From the satellite presentation, Pamela developed substantial deep convection associated with a convective burst near the center between 0600 and 1800 UTC on 11 October. From the longwave

Accepted for publication in *Weather and Forecasting*. DOI 10.1175/WAF-D-22-0194.1.

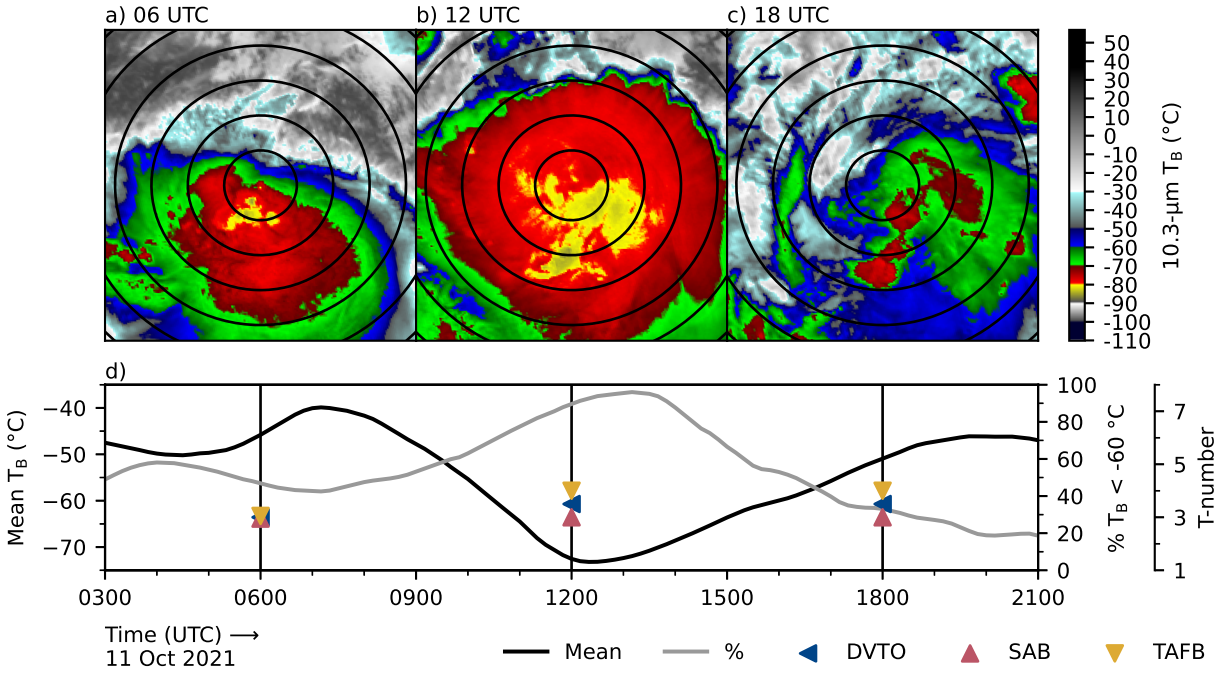

FIG. 1. The evolution of Hurricane Pamela (2021) in the *GOES-16* channel 13 10.3-μm IR brightness temperatures during 11 October. The top row shows storm-centric images for a) 0600, b) 1200, and c) 1800 UTC with 50-km range rings overlaid. The bottom plot d) shows the mean brightness temperature in °C (black curve) averaged from 0 to 200 km in radius, the percent area less than $T_B \leq -60$ °C (gray curve) in the annulus from 50 to 200 km in radius, and the satellite-based final "T-number" values from the NESDIS Satellite Analysis Branch (SAB; red up triangle marker), NHC Tropical Analysis and Forecast Branch (TAFB; yellow down triangle marker), and Automated Dvorak Technique (DVTO; blue left triangle marker).

infrared (IR) imagery from Geostationary Operational Environmental Satellite 16 (*GOES-16*), the mean temperature of the cirrus canopy from 0 to 200 km dropped from near −40 °C to near −75 °C and the percent of pixels less than −60 °C from 50 to 200 km neared 100% as the cirrus canopy expanded during this convective burst as shown in Fig. 1. A key, and likely important, aspect of Pamela's satellite presentation is the evolution of the cloud structure from a "curved band" pattern at 0600 UTC (Fig. 1a) to a "central cold cover" (CCC) pattern at 1200 UTC (Fig. 1b) before returning to a "curved band" pattern at 1800 UTC (Fig. 1c).

Accepted for publication in *Weather and Forecasting*. DOI 10.1175/WAF-D-22-0194.1.

The tropical cyclone cloud patterns are part of the satellite-based storm intensity estimate procedure known as the subjective Dvorak technique (Dvorak 1984)[1]. As a nighttime cloud pattern, central cold cover or "persistent bursting" pattern serves as an alternative to other patterns, namely central dense overcast, curved band, or embedded eye cloud patterns, which typically require visible imagery for detection. Dvorak (1984) describes the CCC pattern as convection that is persistently bursting. This manifests itself as a large cirrus canopy with a long-lived cluster of overshooting convective tops that remain relatively stationary. At the larger scale, the brightness temperatures from 0 to 200 km become almost uniform as ice is ejected by the overshooting convective tops and expands radially outward. While the CCC pattern is infrequently seen, Dvorak noted that this pattern has important implications for intensity trends in that this pattern indicates a slowed or arrested development of the tropical storm (Dvorak 1984; Lander 1999).

Using Hurricane Pamela's suboptimal intensity forecasts as motivation, we want to understand if Pamela represents an outlier case or if the sudden, short-term burst of deep convection emblematic of the CCC pattern represents a possible failure mode for dynamical and statistical–dynamical intensity aids. Here, we use Dvorak patterns routinely labeled by the National Environmental Satellite, Data, and Information Service (NESDIS) Satellite Analysis Branch Tropical Team and Joint Typhoon Warning Center to capture the descriptive characteristics of labeled CCC cases and quantify the duration of CCC patterns in IR images, section 3, and assess the storm environment and skill of intensity guidance during CCC events, section 4.

2. Data

For our investigation, we use storm characteristics from the best-track and forecasts databases, Dvorak fix information, archived storm-centric IR imagery, and model-derived storm environmental information.

a. Best-track and forecast databases

The Automated Tropical Cyclone Forecast (ATCF; Sampson and Schrader 2000) system database has file types to store tropical cyclone history (i.e., best-track file) and forecasts (i.e., a-deck file) from humans, statistic–dynamical aids, deterministic and ensemble numerical weather prediction

[1]Dvorak (1972, 1975) did not have the CCC pattern because the initial technique relied solely on visible imagery. With the inclusion of IR imagery, Dvorak (1984) added the central cold cover pattern.

Accepted for publication in *Weather and Forecasting*. DOI 10.1175/WAF-D-22-0194.1.

models, and persistence and climatology information. We use the best-track data to provide the post-season analysis of the storm through which we use the position and intensity to quantify guidance forecast errors. We note that best-track intensities come from a blend of available information as recently documented by the Joint Typhoon Warning Center (Howell et al. 2022). The National Hurricane Center likely follows a similar procedure, based on a blending of the intensity information from satellite sensors trusted in operations including aircraft reconnaissance-derived intensity information.

From the a-decks, we use forecasts from the Global Forecast System (technique identifier AVNO for "late" and AVNI for "early" or interpolated), Hurricane Weather Research and Forecast (HWRF for "late" and HWFI for "early" or interpolated; Tallapragada et al. 2014; Sampson et al. 2008), Statistical Hurricane/Typhoon Intensity Prediction Scheme (SHIPS/STIPS; DeMaria and Kaplan 1994; Knaff et al. 2005), Logistic Growth Equation Model (LGEM; DeMaria 2009), and 5-day Statistical Hurricane/Typhoon Intensity Forecast climatology and persistence (SHF5/ST5D; Knaff et al. 2003).

b. Dvorak fix data

Operational satellite analysis groups store and disseminate information from the subjective Dvorak technique primarily in two formats: 1) tropical fix satellite weather bulletins and 2) ATCF fix database. For the subjective Dvorak technique, both formats store the date and time, location of the storm, type of satellite data analyzed, and intensity estimation. Also, each format contains a comment or remark section that may contain additional information on how the analyst created the fix. In this section, the analyst may include the Dvorak cloud pattern used in estimating the intensity.

Since the late-1970s, the NESDIS Satellite Analysis Branch Tropical Team has created subjective Dvorak technique estimates of tropical cyclone intensity (Turk and Kusselson 2002). The team stores these analyses in tropical satellite weather bulletins that contain the time of the fix, storm center latitude and longitude, satellite data used to construct the fix, intensity estimate as a tropical and current-intensity number, and a remark section with the cloud pattern. Archived bulletins are publicly available from 2007 to present from the Satellite Products and Services Division of NESDIS. The archive does not include North Atlantic or eastern North Pacific until 2013.

Accepted for publication in *Weather and Forecasting*. DOI 10.1175/WAF-D-22-0194.1.

In addition to the tropical satellite weather bulletins, human analysts store fix data from the NESDIS Satellite Analysis Branch Tropical Team, National Hurricane Center Tropical Analysis and Forecast Branch, and Joint Typhoon Warning Center in the ATCF fix database (f-deck). The fix database contains the storm center latitude and longitude, intensity, wind radii, and central pressure fixes from a variety of human and algorithm inputs that leverage a menagerie of data sources. For satellite analyst Dvorak technique fixes, the fix-deck stores this information under the fix type "subjective Dvorak" (i.e., DVTS). From 2009 onward, the NESDIS Satellite Analysis Branch Tropical Team has always included a specified fix format in the remark section of subjective Dvorak fixes. In 2009, the NESDIS Satellite Analysis Branch Tropical Team standardized the format and cloud pattern coding included a space-delimited structure. From 2010 onward, subjective Dvorak fixes from the NESDIS Satellite Analysis Branch Tropical Team include a specified comment section format that lists the Dvorak pattern type. The Joint Typhoon Warning Center also uses a specified comment section, but the analysts do not code the cloud patterns uniformly in the data from 2011 to present that is available to the authors. The National Hurricane Center Tropical Analysis and Forecast Branch does not routinely use the comment section nor are comments formatted when present.

Unlike the ATCF best-track database, fix information does not go through a post-season analysis to correct any issues. Fortunately (or unfortunately for this work as our focus is on the specific cloud pattern), the analysts have a margin of error when using the subjective Dvorak technique to yield similar tropical and current-intensity numbers if a pattern is misidentified at low storm intensities. We do not take steps to mitigate erroneous Dvorak pattern classifications. We want to convey that this work should not be construed as a robust nor complete climatology of central cold cover. Also, various satellite analysis groups create subjective Dvorak technique fixes at different, but routine times. And, because of the brevity of the central cold cover, we opt to include any central cold cover pattern listed in the fix without trying to interpolate or blend cloud patterns in time. For consistency, we focus on 2011 to 2021 to create a homogeneous sample of Dvorak fix patterns across tropical cyclone basins. Focusing on this period also allows us to stay homogeneous when selecting forecast models to assess forecast skill.

Accepted for publication in *Weather and Forecasting*. DOI 10.1175/WAF-D-22-0194.1.

TABLE 1. Bulk characteristics of subjective Dvorak fixes containing central cold cover, CCC, from 2011 to 2021.

Number of Fixes	176
Percent of Fixes	~0.1%
Average per Year	16
Number of Storms	144
Percent of Storms	13%

c. Geostationary infrared imagery

We use IR imagery from the Regional and Mesoscale Meteorology Branch tropical cyclone IR archive (Knaff et al. 2014). The archive contains global geostationary satellite imagery on a 4- × 4-km grid with approximately 15- to 30-minute resolution and has a central wavelength near 11 μm. Also, we calculate and use two metrics that are similar to what is found in the SHIPS large-scale environment diagnostic developmental data set (RAMMB 2022): 1) the mean brightness temperature averaged from 0 to 200 km in radius around the storm, and 2) percent area less than −60 °C in the annulus from 50 to 200 km in radius.

d. Tropical cyclone environment

To evaluate the tropical cyclone environment during periods with the CCC pattern, we will use numerical weather prediction model-based environmental parameters. For this work, we extract parameters from the SHIPS large-scale environment diagnostic developmental data set (RAMMB 2022). Here, we use the 200- to 850-hPa deep-layer, 500- to 850-hPa shallow-layer, and generalized vertical wind shear metrics, sea surface temperature, 500- to 700-hPa middle tropospheric relative humidity, and vertical mass flux calculated from a one-dimensional cloud model that includes entrainment, condensate weight, and both liquid and ice phases of water (DeMaria 2009).

3. Central cold cover characteristics

To estimate tropical cyclone intensity using the subjective Dvorak technique, satellite analysts locate the storm center and then determine the cloud pattern. For CCC cases from 2011 to 2021, Table 1 shows bulk characteristics for the North Atlantic, western, central, eastern North Pacific, North Indian Ocean, and Southern Hemisphere. From the table, satellite analysts infrequently select CCC relative to the other Dvorak cloud patterns. During the 2011–2021 period, satellite

Accepted for publication in *Weather and Forecasting*. DOI 10.1175/WAF-D-22-0194.1.

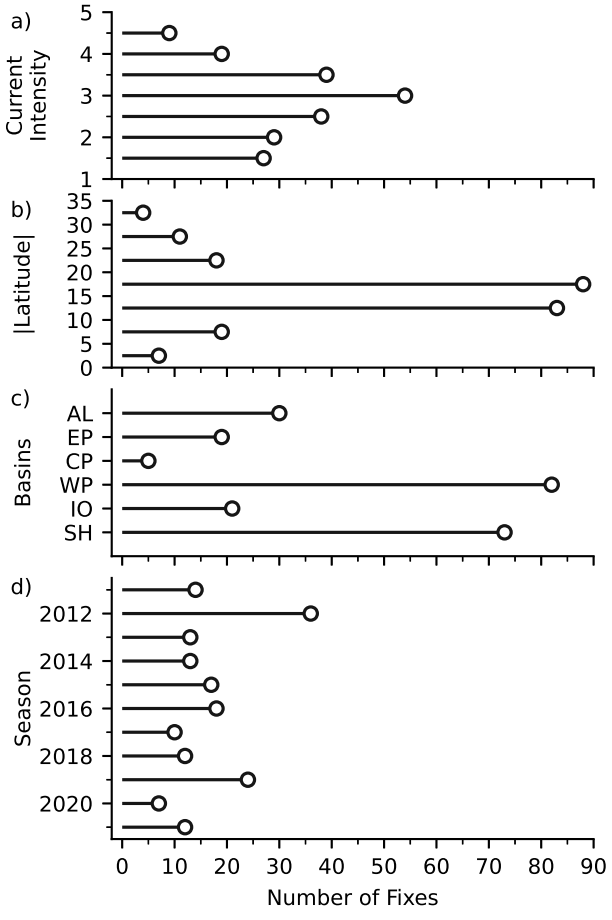

FIG. 2. Central cold cover, CCC, frequency characteristics based on the Subjective Dvorak technique fix information for a) the current intensity number, b) the absolute value of latitude by binned by 5 degrees, c) tropical cyclone ocean basin where AL is the North Atlantic, EP, CP, and WP are the eastern, central, and western North Pacific, IO is the North Indian Ocean, and SH is the Southern Hemisphere, and d) the tropical cyclone season (note that the SH season starts on 1 July of the preceding year).

analysts based the intensity on CCC patterns 176 times, which represents 0.1% of all subjective Dvorak fixes. While relatively rare, satellite analysts use the CCC pattern at least once for 144 (13.4%) of the 1077 numbered tropical cyclones during this period.

Figure 2 shows the frequency from 2011 to 2021 at which satellite analysts base the intensity estimate on the CCC pattern as a function of a) current intensity number, b) absolute latitude, c) basin, and d) season. For the current intensity number in Fig. 2a, we bin based on 0.5 intervals. This figure shows that the CCC pattern is associated with Dvorak current intensity numbers ranging from 1.5 to 4.5 (25 to 77 kt) with a peak between 2.5 and 3.5 (35 to 55 kt). For the latitude in

Accepted for publication in *Weather and Forecasting*. DOI 10.1175/WAF-D-22-0194.1.

Fig. 2b, we bin the central latitude of fixes with CCC patterns at 5-degree latitude intervals. From the figure, the latitudinal distribution of CCC cases is relatively Gaussian with 64% of instances occurring between 10- and 20-degrees latitude with a mean latitude of 15.6 degrees and standard deviation of 5.3 degrees. From a basin perspective, the Southern Hemisphere and western North Pacific have the largest number of fixes based on CCC pattern followed by the North Atlantic as shown in Fig. 2c. From the yearly perspective as shown in Fig. 2d, satellite analysts use CCC relatively consistently with a mean of 16.0 occurrences and a standard deviation of 7.6.

Since the CCC pattern can only be determined using IR imagery (Dvorak 1984), the CCC pattern shares similarities to patterns available to satellite analysts, specifically the central dense overcast pattern. To understand when satellite analysts use the CCC pattern in comparison to the central dense overcast pattern, we use the central longitude from the subjective Dvorak technique to convert the fix time from coordinated universal time to local sidereal time. Figure 3 contains the hourly binned number of fixes shaded on a logarithmic scale containing a) CCC and b) central dense overcast. The inner ring in Fig. 3 indicates local sidereal nighttime (blue) when only IR imagery is available from geostationary satellites and daytime (orange) when visible imagery is also present to determine the cloud pattern. From Fig. 3a, satellite analysts base intensity estimates on the CCC pattern at night with the majority occurring between 2300 and 0300 local sidereal time and use it infrequently during the day. Analysts select central dense overcast, Fig. 3b, during the day, which is to be expected as a visible-only pattern. While CCC is applicable during the day, the comparison between CCC and central dense overcast suggests that features are available during the day that give preference to Dvorak patterns using visible imagery, which is likely preferred historically due to generally higher spatial resolution. We note that Lander (1999) made similar remarks about applications of the CCC pattern. Thus, we believe that the subjective Dvorak technique fix pattern information is not applicable to understanding diurnal cycles in deep convection in tropical cyclones.

From the large-scale presentation in the imagery in Fig. 1a–c, the brightness temperatures from 0 to 200 km become almost uniform as ice is ejected by the overshooting convective tops and expands radially outward. From Fig. 1d, we see the evolution of the mean brightness temperature averaged from 0 to 200 km in radius around the storm (black curve) and percent area less than −60 °C in the annulus from 50 to 200 km in radius (gray curve). For Pamela, the mean average temperature

Accepted for publication in *Weather and Forecasting*. DOI 10.1175/WAF-D-22-0194.1.

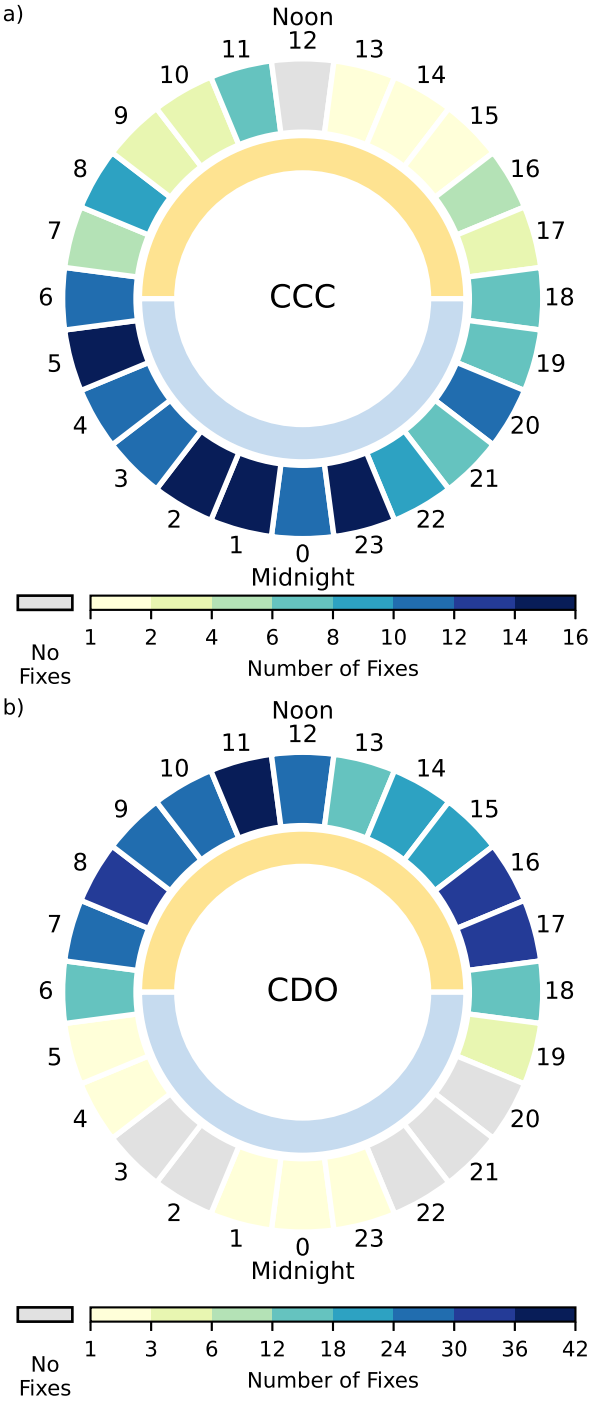

FIG. 3. Subjective Dvorak technique fixes for storms with sustained winds less than 77 kt (1 kt $\approx$ 0.514 m s^{-1}) from 2011 to 2021 based on a) central cold cover (CCC) and b) central dense overcast (CDO). The number of fixes binned by local sidereal time (shading) with local midnight and noon at the bottom and top of the plot, respectively. The inner ring indicates nighttime (blue) and daytime (orange).

Accepted for publication in *Weather and Forecasting*. DOI 10.1175/WAF-D-22-0194.1.

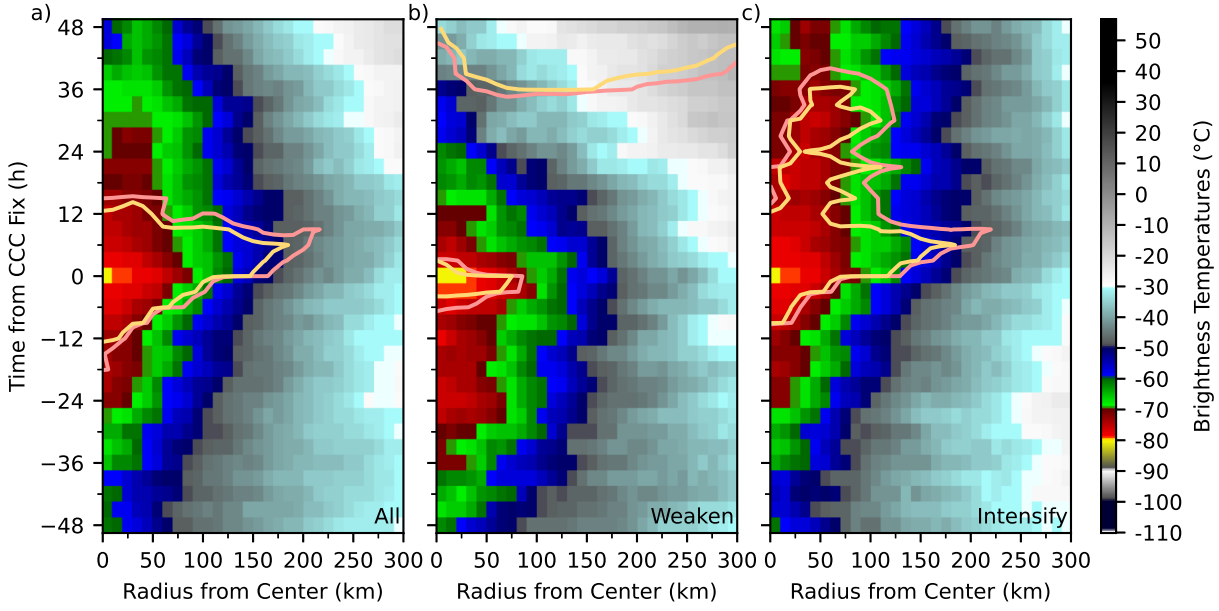

FIG. 4. Hovmöller diagrams of the azimuthal median of the IR brightness temperatures. The brightness temperatures are binned by 10 km in radius out to 300 km and 3 h in time out to ± 48 h centered on the central cold cover (CCC) Dvorak fix for a) all cases at least tropical storm strength (34 kt), b) cases that weaken between $t = 0$ and 48 h, and c) cases that are steady or intensify between $t = 0$ and 48 h. Contours show p values of 5.181×10^{-5} (salmon curve) and 1.015×10^{-5} (tan curve) calculated with a two-sided Mann–Whitney U statistic test that corresponds to having true null hypotheses at the $\alpha_0 = 0.05, 0.01$ levels.

reaches a minimum while the percent area continues to increase as the deep-convective pulsing from overshooting tops ends, but the cirrus cloud shield continues to expand and cool. After the CCC behavior has ended, the scene warms, reflecting the general lack of convection as the storm attempts to reorganize, Fig. 1c.

To see if Pamela's evolution is the typical behavior for CCC pattern, we take the median of brightness temperatures for each case in 3-h intervals out to 48 hours before and after the central cold cover label by a satellite analyst out to 300 km at 10-km radial intervals. At the time of the fix, the system must have a current intensity of 34 kt (i.e., tropical storm strength) or greater and the system must persist in the best-track file for 48 h after the fix. In Fig. 4, we show Hovmöller diagrams of the azimuthal median of the brightness temperatures for a) all 127 cases matching our criteria, b) the 46 cases that weaken between $t = 0$ and 48 h (a mean weakening of ~ 30 kt in 48-h) and c) the 68 cases that intensify between $t = 0$ and 48 h (a mean intensification of

Accepted for publication in *Weather and Forecasting*. DOI 10.1175/WAF-D-22-0194.1.

$\sim$ 20 kt in 48-h; note that the 13 steady-state cases are not shown but are the same evolution as intensifying). To evaluate where the radial brightness temperature profiles for CCC cases deviate from typical storms, we calculate the distribution of brightness temperature for each radial bin for over 210 000 storm-centric images with initial intensities between 34 and 127 kt (T-numbers 2.5 to 6.5; expanded beyond the CCC intensity distribution to include the T-number range associated with the mean 48 h intensification) and the absolute value of latitude values between 10.3 and 20.9 degrees, which is one standard deviation from the mean latitude of CCC cases. Using these "low-latitude" brightness temperature distributions, we perform a two-sided Mann–Whitney U-statistic test (Mann and Whitney 1947) on each composite pixel. In conducting multiple significance tests, we use Walker's criterion to define a stricter threshold for assessing significance to reduce the number of false rejections of the null hypothesis (Katz 2002; Wilks 2016). To determine which point deviates from the low-latitude radial distribution, we contour p values in Fig. 4 that equal Walker's criterion values of $\alpha_{\text{Walker}} = 1-(1-\alpha_0)^{1/N_0} = 5.181\times10^{-5}, 1.015\times10^{-5}$, where the overall significance levels are $\alpha_0 = 0.05, 0.01$, and the total number of true null hypotheses is $N_0 = 990$. We can reject the null hypothesis near the storm center around the period of the CCC, which highlights the abruptness in which the CCC pattern occurs and deviates from typical brightness temperature values.

Across all cases, the brightness temperature values are less than -70 °C for roughly 12 to 18 h centered on the fix. In the weakening cases (Fig. 4b), the brightness temperatures prior to $t = 0$ show more of a diurnal oscillation as shown by a short period of brightness temperature values less than -70 °C in the 24 h prior to the central cold cover fix. For intensifying cases (Fig. 4c), the brightness temperatures are warm prior to the development of the CCC pattern. From the weakening and intensifying cases, there seems to be a pattern prior to CCC that is suggestive of the post-CCC intensity trend. Given that the CCC pattern is predominately at night, this observed oscillation in brightness temperature is consistent with the typical diurnal oscillation observed in the majority of tropical cyclones (Knaff et al. 2019).

To understand the spatial structure, we examine the two-dimensional structure at $t = -24, 0, 24$ h using 10-km radial by 10-degree azimuthal bins to calculate the median of the IR brightness temperatures for all, weakening, and intensifying cases. In Fig. 5, the bottom row shows the composites at $t = -24$ h, the middle shows $t = 0$ h, and the top shows $t = 24$ h with the left column

Accepted for publication in *Weather and Forecasting*. DOI 10.1175/WAF-D-22-0194.1.

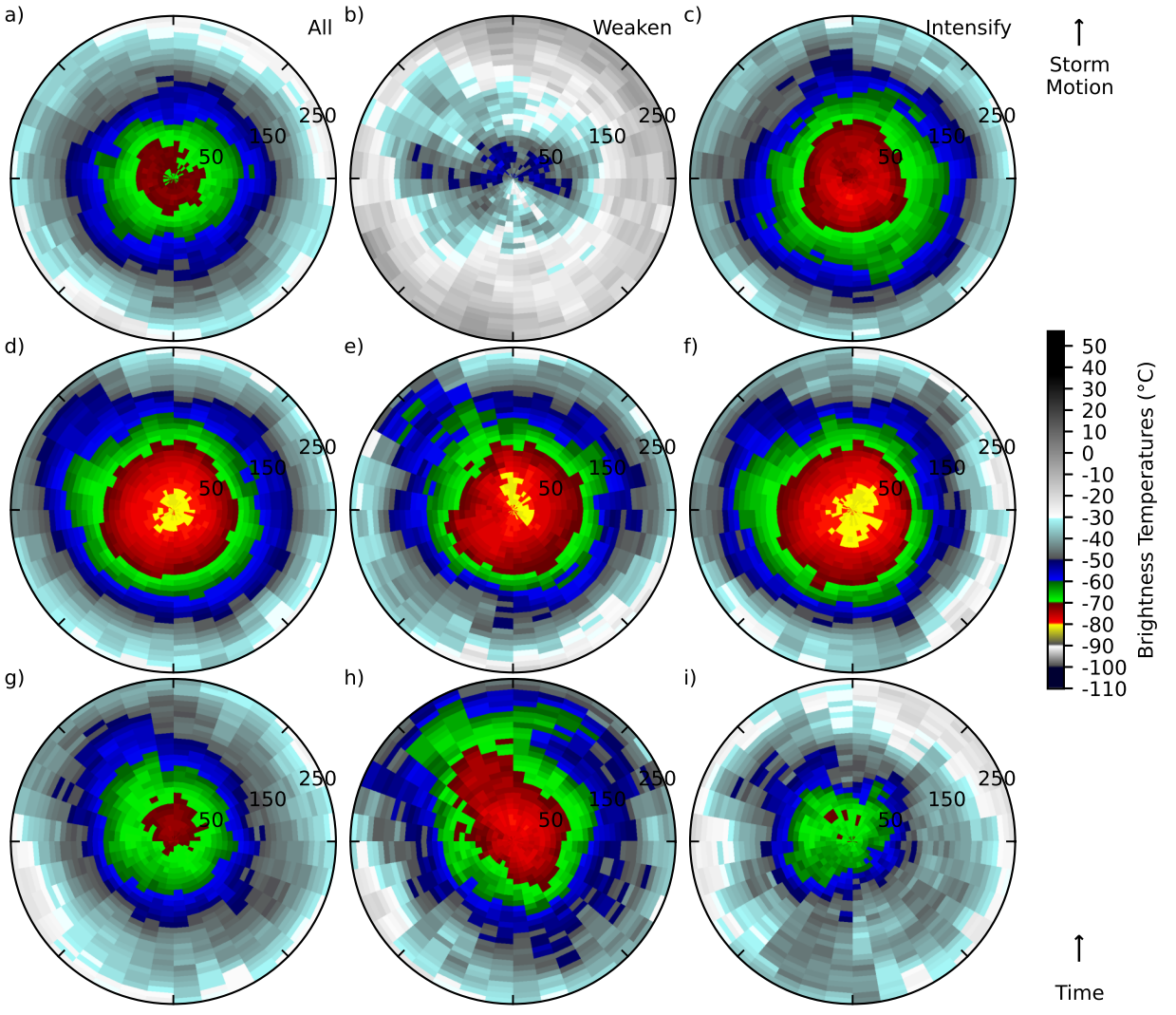

FIG. 5. Storm-motion oriented, two-dimensional median of IR brightness temperatures binned to a 10-km radius out to 300 km by 10-degree azimuth grid for all central cold cover cases (left column), storms that weaken 48-h after central cold cover (middle column), and storms that intensify 48-h (right column) at $t = -24$ h (bottom row), $t = 0$ h (middle row), and $t = 24$ h (top row).

showing all CCC cases, middle showing weakening and right showing intensifying. Figure 5 highlights a few details that cannot be gleaned from the Hovmöller diagrams. At $t = 0$ h (Figs. 5d–f), the IR satellite presentations are rather homogeneous. But, entering into the CCC period (Figs. 5g–i), the weakening cases show a more asymmetric pattern with convection ahead and to the left of the storm center where the intensifying cases are symmetric and much warmer. When

Accepted for publication in *Weather and Forecasting*. DOI 10.1175/WAF-D-22-0194.1.

exiting the CCC period at $t = 24$ h (Figs. 5a–c), the intensifying cases show the start of eyewall formation while the weakening cases are devoid of deep convection and only the remnants of the cirrus canopy remain.

4. Intensity change

Tropical cyclones change intensity in response to the synoptic-scale environment and internal mechanisms (Ooyama 1982). Because the synoptic-scale environment often dominates, statistical–dynamical intensity aids leverage parameters indicative of the environment. And, to capture internal mechanisms, the statistical–dynamical intensity aids use several IR metrics. To understand the impact of both during CCC periods, we use the SHIPS developmental dataset to calculate the 25th, 50th, and 75th percentiles of various parameters. Table 2 contains these values for the CCC cases (top line per parameter) and low-latitude cases from section 3 (bottom line) for shallow-layer, deep-layer, and generalized vertical wind shear, sea surface temperature (SST), middle-tropospheric relative humidity (RH), and vertical mass flux in the top portion of the table, and the percent area with IR brightness temperature, $T_B \leq -20, -30, -40, -50, -60$ °C, and the current intensity times the standard deviation of the brightness temperature between 0 to 200 km in the bottom portion of the table. We use a two-sided Mann–Whitney U-statistic test (Mann and Whitney 1947) to determine whether the variable distribution for central cold cover cases is statistically different from cases occurring at low-latitude cases or, in this case, between 10.3 and 20.9° latitude where the majority of CCC cases occur (see Fig. 2). We reject the null hypothesis to the 99% confidence level ($\alpha = 0.01$) that the environment for the two sets of cases are the same for sea surface temperature and vertical mass flux (in italics in Table 2) and all IR brightness temperature thresholds. The warm sea surface temperatures and favorable thermodynamic profile as indicated by high vertical mass flux values are indicators of future intensification as well as large areas with cold brightness temperatures. And, the other parameters are typical for systems that tend to continue to develop.

With conditions indicative of intensification as seen in Pamela, we explore if storms exhibiting other CCC periods also have higher than normal intensity forecast errors. To understand intensity errors during CCC, we create a homogeneous subset of the 2011 to 2021 intensity forecasts from the SHF5, AVNI, HWFI, DSHP, and LGEM for cases that have an initial intensity above 34 kt and do not make landfall during the 48-h forecast period, which drops our total number of CCC

Accepted for publication in *Weather and Forecasting*. DOI 10.1175/WAF-D-22-0194.1.

TABLE 2. The interquartile range and median of large-scale tropical cyclone environmental conditions and longwave infrared during central cold cover periods (top row per parameter) and low-latitude cases (bottom row). The top portion of the table contains the 850- to 500-hPa shallow-layer, 850- to 200-hPa deep-layer, and generalized vertical wind shear metrics, sea surface temperature (SST), middle-tropospheric relative humidity and vertical mass flux calculated from a one-dimensional cloud model. The bottom portion of the table contains percent area between 50 and 200 km in radius with brightness temperatures, $T_B \leq -20, -30, -40, -50, -60$ °C (PC20, PC30, PC40, PC50, PC60, respectively), and current intensity times the standard deviation of the brightness temperatures between 0 and 200 km (VIRSD). The asterisk for the large-scale environmental conditions and all longwave infrared thresholds indicates that the null hypothesis that conditions between the two sets of cases have been rejected using a Mann–Whitney U-statistic test at the 99% confidence level (i.e., the p value is less than $\alpha = 0.01$).

Parameter	Units	Percentile		
		25th	50th	75th
Large-scale Environment				
Shallow-layer Shear	kt	4.0	6.5	9.0
		4.0	6.4	9.5
Deep-layer Shear	kt	9.5	14.2	20.2
		8.7	13.4	19.0
Generalized Shear	kt	17.8	23.1	29.7
		16.8	21.9	28.7
SST *	°C	28.5	29.0	29.6
		27.8	28.8	29.5
Relative Humidity	%	57	65	74
		56	65	73
Vertical Mass Flux *	m s^{-1}	4.9	6.2	7.7
		3.3	5.5	7.5
Longwave Infrared Predictors				
PC20 *	%	69.8	87.5	99.0
		60.0	83.0	96.0
PC30 *	%	57.8	81.5	97.0
		51.0	74.0	90.0
PC40 *	%	51.0	74.0	93.0
		42.0	64.0	83.0
PC50 *	%	41.5	63.5	88.3
		31.0	51.0	72.0
PC60 *	%	29.8	51.0	75.3
		17.0	35.0	55.0
VIRSD *	kt °C	381	572	841
		518	697	905

Accepted for publication in *Weather and Forecasting*. DOI 10.1175/WAF-D-22-0194.1.

cases from 176 to 62, 54, 51, and 47 for the 12-, 24-, 36-, and 48-h forecast, respectively. The average intensity change for these forecast periods is 5.5, 9.6, 12.4, 17.8 kt in 12, 24, 36, and 48 h, respectively. While not discussed here, note that the findings are the same for an inhomogeneous sample of non-landfalling storms. Based on the bulk characteristics shown in Fig. 2, we subset all CCC forecasts. As in the previous section, we define a subset that we refer to as "low-latitude cases" as ones that are non-landfalling, contain storms with initial intensities between 34 and 77 kt and the absolute value of latitude values between 10.3 and 20.9 degrees, which is one standard deviation from the mean latitude of CCC cases.

Figure 6 shows the forecast intensity errors (top row) and skill relative to SHF5 (bottom row) for CCC (left column) and all low-latitude cases (right column) for the 12-, 24-, 36-, and 48-h forecast periods. For CCC cases, SHF5 (black curve with circle marker) has just slightly larger intensity errors (12–36 h) relative to the low-latitude cases as shown in Figs. 6a–b. And, the intensity guidance for the CCC cases is also worse than in low-latitude cases. Despite the CCC cases being more difficult to forecast as indicated by the larger SHF5 errors, the net impact of the two is that skill relative to SHF5 for central cold cover is significantly degraded with respect to other cases as shown in Figs. 6c–d. This holds true for each forecast guidance technique. While degraded, HWFI (cyan curve with diamond marker) appears to have a slight advantage over other intensity forecast aids in that the skill of the model for both mean absolute error and root-mean-square error remains positive during the CCC cases except for 48-h forecasts. AVNI (blue curve with square markers) struggles to resolve weak vortices, which likely accounts for similar skill in the 12- and 24-h forecast periods. The statistical–dynamical models DSHP (orange curve with down triangle marker) and LGEM (red curve with up triangle marker) perform similarly and struggle to improve skill over SHF5 in the CCC cases. While not shown, we also calculated the mean bias error for all techniques. The intensity bias is approximately ±5 kt at 24 h and ±10 kt with no discernible signal, which might reflect changes to the guidance from season to season.

While we tried to compare the CCC cases to similar storms, random chance given our sample size can explain some amount of the skill difference relative to climatology and persistence. To understand the degree to which random chance might impact our comparison, we take random bootstrap samples from our low-latitude cases between 35 and 75 kt. Each bootstrap sample is the size of each 12-h forecast period (i.e., 62, 54, 51, and 47 respectively) and we create 100 000

Accepted for publication in *Weather and Forecasting*. DOI 10.1175/WAF-D-22-0194.1.

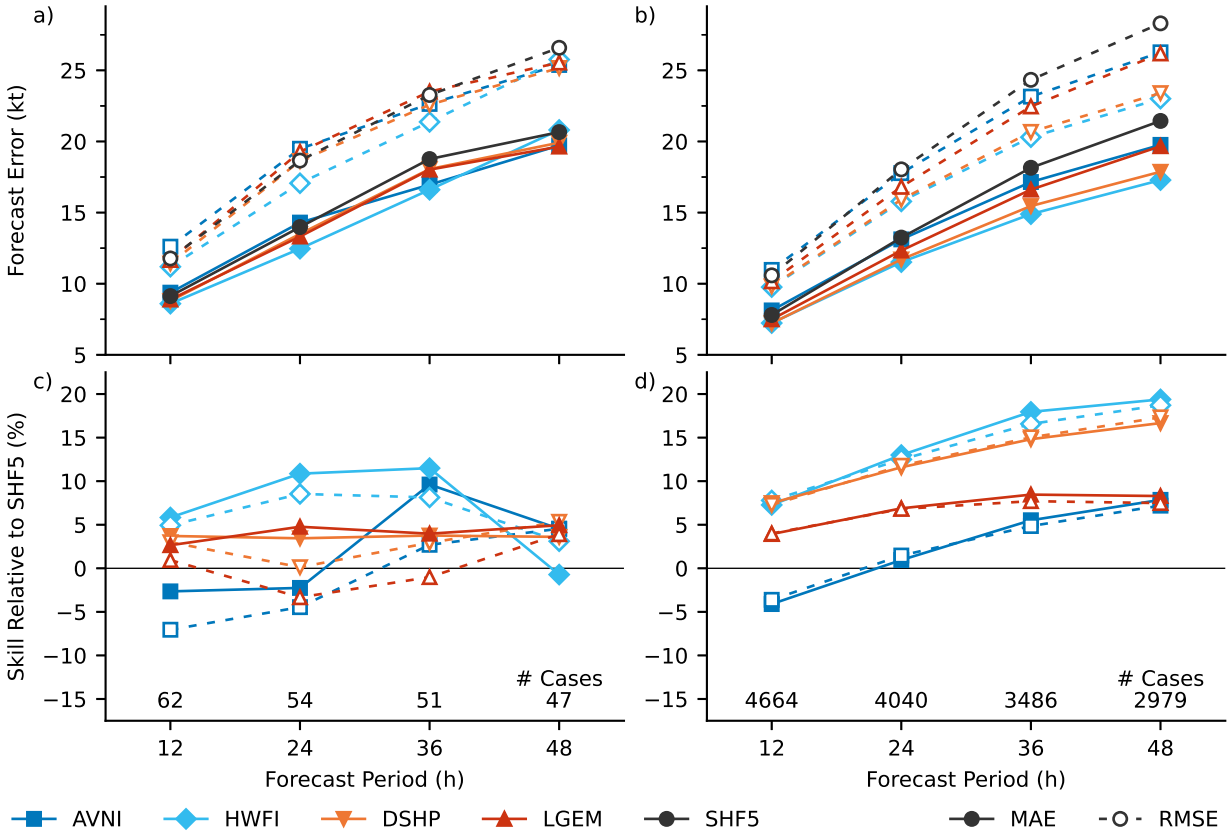

FIG. 6. The 2011 to 2021 forecast intensity errors in kt (top row) and skill relative to climatology and persistence, SHF5, (bottom row) for the central cold cover cases (left column) and low-latitude cases between 35 and 75 kt and percent skill relative to SHF5 (right column) for the 12-, 24-, 36-, and 48-h forecast periods. Mean absolute error (MAE) is in the solid curve with the closed marker and root-mean-square error (RMSE) is in the dashed curve with an open marker for the Global Forecast System (AVNI; blue curve with square marker), Hurricane WRF (HWFI; cyan curve with diamond marker), Decay-SHIPS (DHSP; orange curve with down triangle marker), LGEM (red curve with up triangle marker), and 5-day persistence and climatology (SHF5; black curve with circle marker).

permutations per forecast period—we also tried creating season-isolating permutations to emulate the approach in DeMaria et al. (2014) and Trabing and Bell (2020) and see similar results. For each permutation, we determine whether the sample has a worse root-mean-square error skill relative to our CCC cases (Fig. 6c). For the 12-, 24-, 36-, and 48-h forecast periods, we plot the percentage of forecasts worse than the root-mean-square error skill in Fig. 7. From this analysis, we see that CCC
364 case intensity forecasts are among the worst for the statistical–dynamical models with performance

Accepted for publication in *Weather and Forecasting*. DOI 10.1175/WAF-D-22-0194.1.

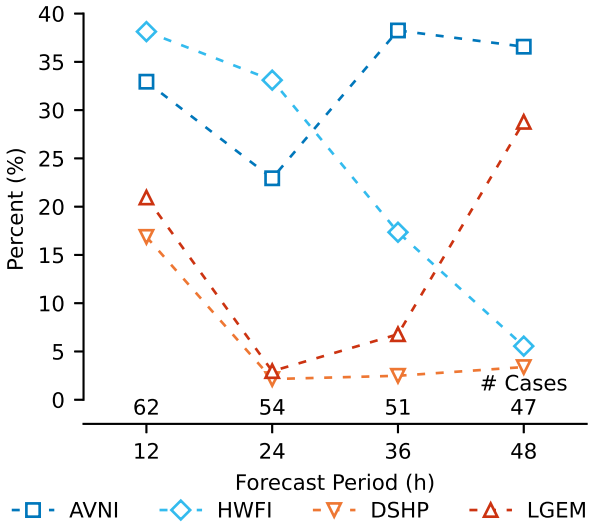

FIG. 7. The percent of 100 000 bootstrap random permutations per model for low-latitude cases between 35 and 75 kt where the root-mean-square error skill is worse than the root-mean-square error skill for central cold cover. The size of each individual bootstrap permutation is labeled as the number of cases (62, 54, 51, 47) for each forecast period (12, 24, 36, 48 h), respectively. The models are the Global Forecast System (AVNI; blue curve with square marker), Hurricane WRF (HWFI; cyan curve with diamond marker), Decay-SHIPS (DHSP; orange curve with down triangle marker), and LGEM (red curve with up triangle marker).

dropping from near 20% to less than 5% for the 12- and 24-h forecasts, respectively, which aligns with the favorable environmental conditions (Table 2) and cold brightness temperatures. For the dynamical models, AVNI shows no substantial performance change between the CCC cases and low-latitude cases. The performance of AVNI is consistent with model's tendency to poorly resolve weak systems. HWFI intensity forecasts performance degrades over the 48-h period, which might indicate an unrealistic spin up of the model convection when compared to nature.

Given the impact of CCC to infrared-based predictors, a natural question is how much do the pixel counts affect intensity forecasts from statistical–dynamical guidance for tropical cyclone intensity change and rapid intensification probabilities? For intensity, we can examine the 24-h normalized coefficients of two IR predictors in SHIPS models run at NHC and JTWC. All SHIPS models use the percentage of pixels less than 20 °C within a 50- to 200-km annulus ($T_B \leq 20$ °C; PC20) and the current intensity times the brightness temperature standard deviations within the 0- to 200-km annulus (VIRSD). The 24-h normalized coefficients, their means (μ) and standard

Accepted for publication in *Weather and Forecasting*. DOI 10.1175/WAF-D-22-0194.1.

deviations (σ), the mean 24-h mean intensity changes and standard deviations of those changes were obtained for the latest model fits at NHC (Mark DeMaria, personal communication 2023) and JTWC (Buck Sampson, personal communication 2023). This allows us to calculate the 24-h intensity change sensitivities to a one-sigma change in both of the predictors. These statistics and the small resulting changes are shown in Table 3 for the western North Pacific, Southern Hemisphere, North Atlantic and eastern North Pacific in terms of kt of intensity change and percentage of the climatological intensity change. During CCC these predictors are typically anti-correlated with the PC20 increasing and the VIRSD decreasing. When other predictors are held constant, the combined impact of a one sigma change to these predictors is a relatively small ~0.4 kt increase at 24-h or about 2.2% of the mean 24-h intensity change globally and has the largest impact in the northwest Pacific. Similar one-sigma increases in IR predictors used for estimating rapid intensification probabilities, on the other hand, have a much larger impact because the normalized coefficients in these schemes are typically at least an order of magnitude larger (e.g., Knaff et al. 2020; Kaplan et al. 2010), and in a marginal rapid intensification, the environment could ultimately change the yes/no answer. In fact, one sigma changes in the pixel counts, the percentage of pixels less than 50 °C within a 50- to 200-km annulus in Knaff et al. (2020) would result in 31% and 58% increase in rapid intensification (30 kt in 24 h) probabilities above the rapid intensification climatology in the linear discriminant analysis and logistic regression formulations, respectively.

5. Discussion and Conclusion

While the intensity forecast errors are larger than typical, Hurricane Pamela (2021) is not unique in having large forecast intensity errors after exhibiting the CCC cloud pattern. As outlined, the majority of tropical cyclones arrest in development for 12 to 24 hours after exhibiting the CCC pattern as noted by Dvorak (1984). As shown here, tropical systems exhibit CCC characteristics for a relatively brief period that is not characteristic of other cloud clusters with large, cold cirrus canopies. Lander (1999) compares CCC patterns to mesoscale convective systems and tropical cloud clusters. However, as the author notes, phenomena like mesoscale convective systems persist longer than the CCC pattern in tropical systems. In some aspects, central cold cover is akin to the convective maximum at the beginning of "stage one" for tropical cyclogenesis documented by Zehr (1992). For tropical cyclogenesis, the systems either exit the short-lived "stage one"-like convective

Accepted for publication in *Weather and Forecasting*. DOI 10.1175/WAF-D-22-0194.1.

TABLE 3. Twenty-four-hour SHIPS IR predictor details are shown. Predictors include the percent area between 50 and 200 km in radius with brightness temperatures, $T_B \leq -20$ °C (PC20) and current intensity times the standard deviation of the brightness temperatures between 0 and 200 km (VIRSD) for each basin-specific SHIPS model. The following columns provided the normalized regression coefficient, the sample predictor's mean value μ in % and kt °C respectively, the sample predictor's standard deviation σ, the model's mean 24-h intensity change μ (intercept), the model's mean 24-h standard deviation σ, the model's response to a one sigma change in the predictor in kt, and the percentage intensity with respect to the mean 24-h intensity change.

Predictor	Normalized Coefficient	Predictor μ	Predictor σ	Intensity Change μ (kt)	Intensity Change σ (kt)	Predicted Intensity Change (kt)	Percent Intensity Change (%)
			Western North Pacific				
PC20	0.037	81.2	19.6	20.0	5.48	0.20	1.00
VIRSD	−0.078	738.	327.	20.0	5.48	−0.43	−2.15
			Southern Hemisphere				
PC20	0.069	76.2	24.2	19.9	3.10	0.21	1.06
VIRSD	−0.079	657.	285.	19.9	3.10	−0.25	−1.26
			North Atlantic				
PC20	0.054	63.8	27.1	15.4	4.28	0.23	1.48
VIRSD	−0.022	833.	353.	15.4	4.28	−0.10	−0.65
			Eastern North Pacific				
PC20	0.068	70.1	27.2	19.3	1.54	0.11	0.57
VIRSD	−0.022	833.	353.	19.3	1.54	−0.12	−0.62

maximum to further develop or dissipate. In CCC cases, systems exit arrested development having had convection contribute constructive or destructive for further development.

The CCC pattern appears to have a diurnal behavior as illustrated above in Figs. 3–5. The loss of visible imagery at night is likely one reason for this behavior, but there is also a tendency for deep convection in tropical cyclones to beat diurnally. Dunion et al. (2014) ushered in a resurgence in understanding diurnal aspects of convection and the cirrus canopy in intense tropical cyclones. Both Knaff et al. (2019) and Ditchek et al. (2019) highlight that weaker systems like tropical storms and weak hurricanes exhibit a diurnal cycle in the IR imagery. Understanding how the CCC cloud pattern fits within the tropical cyclone diurnal cycle literature is natural. One possible thought is that CCC patterns that occur in the early morning hours are failed diurnal cycles with rapid deterioration of the cold cloud canopy after the start of the intense convection. But, as we

Accepted for publication in *Weather and Forecasting*. DOI 10.1175/WAF-D-22-0194.1.

suggested in the context of Fig. 3, we do not think that significance can be placed on when the CCC pattern occurs during the day.

The subjective identification of CCC patterns based on "bursting" also likely adversely affects objective techniques patterned after Dvorak's Technique. Because of the frequency of CCC in the fix data and similarity of the pattern, operational algorithms such as the automated Dvorak technique (Velden et al. 1998, 2006) do not incorporate the CCC pattern as a unique cloud pattern type. Because of this and the impact that CCC has on the short-term forecast skill, we recommend that forecasters remain cognizant of the cloud pattern from subjective Dvorak technique fixes for systems between T-number 1.5 and 4.5 as well as the intensity trend advised for CCC occurrences in Dvorak (1984).

This study was only possible due to the serendipitous common formatting of comments in the ATCF fix data, namely from both the Joint Typhoon Warning Center and NESDIS's Satellite Analysis Branch. From this work, the Dvorak cloud pattern is useful for diagnosing possible failure modes in the tropical cyclone intensity guidance and an analysis of the other cloud patterns may provide other useful insights at critical times in the tropical cyclone life cycle. We would also recommend that satellite analysis groups elsewhere adopt the same specified comment and remark system for the subjective Dvorak technique and use consistent cloud pattern coding so that the research and developer communities can fully examine forecast failure modes and other aspects of tropical cyclone behavior that benefit from an analyst's eyes.

The CCC pattern is indeed related to arrested development and intensity forecast uncertainty, which leads to several unanswered questions. Can the CCC pattern be objectively identified? If so, is there sufficient data to unravel any potential relationship between CCC occurrence and diurnal aspects of tropical cyclone convection and differences between cases where the tropical cyclone persists or dissipates? And, does accounting for CCC patterns improve intensity forecasts?

Acknowledgments. The authors would like to thank two anonymous reviewers as well as Ben Trabing and Mark DeMaria for their comments on an early version of this manuscript as well as the regular attendees for the daily tropical weather briefings at CIRA Fort Collins that spurred a discussion around Hurricane Pamela (2021) in the eastern North Pacific Ocean and led to this manuscript in addition to their employer, NOAA Center for Satellite Applications and Research, for supporting this work. The authors would also like to acknowledge Mark Lander, posthumously, and

Accepted for publication in *Weather and Forecasting*. DOI 10.1175/WAF-D-22-0194.1.

Roger Edson for initiating many discussions of central cloud cover cases and offering operational perspectives to the community via the Tropical Storms mailing list. The scientific results and conclusions, as well as any views or opinions expressed herein, are those of the author(s) and do not necessarily reflect those of NOAA or the Department of Commerce.

Data availability statement. Automated Tropical Cyclone Forecast system (ATCF; Sampson and Schrader 2000) best-track and aid-deck database files are available for the North Atlantic and eastern and central North Pacific at `https://ftp.nhc.noaa.gov/atcf/` and for the western North Pacific, Indian Ocean, and Southern Hemisphere at `https://pzal.metoc.navy.mil/`. NESDIS subjective Dvorak fix information is available in tropical fix satellite weather bulletin format at `https://www.ospo.noaa.gov/Products/ocean/tropical/bulletins.html` and ATCF fix-deck database format at `https://ftp.nhc.noaa.gov/atcf/`.

References

Cangialosi, J. P., 2021: Hurricane Pamela (EP162021). Natl. Hurricane Center Trop. Cyclone Rep., NOAA, Miami, FL, 17 pp.

DeMaria, M., 2009: A simplified dynamical system for tropical cyclone intensity prediction. *Mon. Wea. Rev.*, **137**, 68–82, https://doi.org/10.1175/2008MWR2513.1.

DeMaria, M., and J. Kaplan, 1994: A Statistical Hurricane Intensity Prediction Scheme (SHIPS) for the Atlantic basin. *Wea. Forecasting*, **9**, 209–220, https://doi.org/10.1175/1520-0434(1994)009⟨0209:ASHIPS⟩2.0.CO;2.

DeMaria, M., C. R. Sampson, J. A. Knaff, and K. D. Musgrave, 2014: Is tropical cyclone intensity guidance improving? *Bull. Amer. Meteor. Soc.*, **95**, 387–398, https://doi.org/10.1175/BAMS-D-12-00240.1.

Ditchek, S. D., J. Molinari, K. L. Corbosiero, and R. G. Fovell, 2019: An objective climatology of tropical cyclone diurnal pulses in the Atlantic basin. *Mon. Wea. Rev.*, **147**, 591–605, https://doi.org/10.1175/MWR-D-18-0368.1.

Dunion, J. P., C. D. Thorncroft, and C. S. Velden, 2014: The tropical cyclone diurnal cycle of mature hurricanes. *Mon. Wea. Rev.*, **142**, 3900–3919, https://doi.org/10.1175/MWR-D-13-00191.1.

Accepted for publication in *Weather and Forecasting*. DOI 10.1175/WAF-D-22-0194.1.

Dvorak, V. F., 1972: A technique for the analysis and forecasting of tropical cyclone intensities from satellite pictures. NOAA Tech. Rep. ESS 36, NOAA, Washington, D.C., 15 pp.

Dvorak, V. F., 1975: Tropical cyclone intensity analysis and forecasting from satellite imagery. *Mon. Wea. Rev.*, **103**, 420–430, https://doi.org/10.1175/1520-0493(1975)103⟨0420:TCIAAF⟩2.0.CO;2.

Dvorak, V. F., 1984: Tropical cyclone intensity analysis using satellite data. NOAA Tech. Rep. 11, NOAA, Washington, D.C., 45 pp.

Howell, B., S. Egan, and C. Fine, 2022: Application of microwave space-based environmental monitoring (SBEM) data for operational tropical cyclone intensity estimation at the Joint Typhoon Warning Center. *Bull. Amer. Meteor. Soc.*, in press, https://doi.org/10.1175/BAMS-D-21-0180.1.

Kaplan, J., M. DeMaria, and J. A. Knaff, 2010: A revised tropical cyclone rapid intensification index for the Atlantic and eastern North Pacific basins. *Wea. Forecasting*, **25**, 220–241, https://doi.org/10.1175/2009WAF2222280.1.

Katz, R. W., 2002: Sir gilbert walker and a connection between El Niño and statistics. *Stat. Sci.*, **17**, 97–112, https://doi.org/10.1214/ss/1023799000.

Knaff, J. A., M. DeMaria, C. R. Sampson, and J. M. Gross, 2003: Statistical, 5-day tropical cyclone intensity forecasts derived from climatology and persistence. *Wea. Forecasting*, **18**, 80–92, https://doi.org/10.1175/1520-0434(2003)018⟨0080:SDTCIF⟩2.0.CO;2.

Knaff, J. A., S. P. Longmore, and D. A. Molenar, 2014: An objective satellite-based tropical cyclone size climatology. *J. Climate*, **27**, 455–476, https://doi.org/10.1175/JCLI-D-13-00096.1.

Knaff, J. A., C. R. Sampson, and M. DeMaria, 2005: An operational Statistical Typhoon Intensity Prediction Scheme for the western North Pacific. *Wea. Forecasting*, **20**, 688–699, https://doi.org/10.1175/WAF863.1.

Knaff, J. A., C. R. Sampson, and B. R. Strahl, 2020: A tropical cyclone rapid intensification prediction aid for the joint typhoon warning center's areas of responsibility. *Wea. Forecasting*, **35**, 1173–1185, https://doi.org/10.1175/WAF-D-19-0228.1.

Accepted for publication in *Weather and Forecasting*. DOI 10.1175/WAF-D-22-0194.1.

Knaff, J. A., C. J. Slocum, and K. D. Musgrave, 2019: Quantification and exploration of diurnal oscillations in tropical cyclones. *Mon. Wea. Rev.*, **147**, 2105–2121, https://doi.org/10.1175/MWR-D-18-0379.1.

Lander, M. A., 1999: A tropical cyclone with an enormous central cold cover. *Mon. Wea. Rev.*, **127**, 132–136, https://doi.org/10.1175/1520-0493(1999)127⟨0132:ATCWAE⟩2.0.CO;2.

Mann, H. B., and D. R. Whitney, 1947: On a test of whether one of two random variables is stochastically larger than the other. *Ann. Stat.*, **18**, 50–60, https://doi.org/10.1214/aoms/1177730491.

Ooyama, K. V., 1982: Conceptual evolution of the theory and modeling of the tropical cyclone. *J. Meteor. Soc. Japan*, **60**, 369–380, https://doi.org/10.2151/jmsj1965.60.1_369.

RAMMB, 2022: SHIPS developmental data. Regional and Mesoscale Meteorology Branch, Cooperative Institute for Research in the Atmosphere, Colorado State University, http://rammb.cira.colostate.edu/research/tropical_cyclones/ships/developmental_data.asp.

Sampson, C. R., J. L. Franklin, J. A. Knaff, and M. DeMaria, 2008: Experiments with a simple tropical cyclone intensity consensus. *Wea. Forecasting*, **23**, 304–312, https://doi.org/10.1175/2007WAF2007028.1.

Sampson, C. R., and A. J. Schrader, 2000: The Automated Tropical Cyclone Forecasting System (Version 3.2). *Bull. Amer. Meteor. Soc.*, **81**, 1231–1240, https://doi.org/10.1175/1520-0477(2000)081⟨1231:TATCFS⟩2.3.CO;2.

Tallapragada, V., C. Kieu, Y. Kwon, S. Trahan, Q. Liu, Z. Zhang, and I.-H. Kwon, 2014: Evaluation of storm structure from the operational HWRF during 2012 implementation. *Mon. Wea. Rev.*, **142**, 4308–4325, https://doi.org/10.1175/MWR-D-13-00010.1.

Trabing, B. C., and M. M. Bell, 2020: Understanding error distributions of hurricane intensity forecasts during rapid intensity changes. *Wea. Forecasting*, **35**, 2219–2234, https://doi.org/10.1175/WAF-D-19-0253.1.

Turk, M. A., and S. J. Kusselson, 2002: Aspects of the tropical cyclone program of NOAA/NESDIS. Extended Abstracts, *25th Conf. on Hurricanes and Tropical Meteorology*, San Diego, CA, Amer. Meteor. Soc., P1.9, https://ams.confex.com/ams/pdfpapers/34638.pdf.

Accepted for publication in *Weather and Forecasting*. DOI 10.1175/WAF-D-22-0194.1.

Velden, C., and Coauthors, 2006: The Dvorak tropical cyclone intensity estimation technique: A satellite-based method that has endured for over 30 years. *Bull. Amer. Meteor. Soc.*, **87**, 1195–1210, https://doi.org/10.1175/BAMS-87-9-1195.

Velden, C. S., T. L. Olander, and R. M. Zehr, 1998: Development of an objective scheme to estimate tropical cyclone intensity from digital geostationary satellite infrared imagery. *Wea. Forecasting*, **13**, 172–186, https://doi.org/10.1175/1520-0434(1998)013⟨0172:DOAOST⟩2.0.CO;2.

Wilks, D. S., 2016: "The stippling shows statistically significant grid points": How research results are routinely overstated and overinterpreted, and what to do about it. *Bull. Amer. Meteor. Soc.*, **97**, 2263–2273, https://doi.org/10.1175/BAMS-D-15-00267.1.

Zehr, R. M., 1992: Tropical cyclogenesis in the western North Pacific. NOAA Tech. Rep. 61, NOAA, Washington, D.C., 181 pp.

Accepted for publication in *Weather and Forecasting*. DOI 10.1175/WAF-D-22-0194.1.